DALTON
FULL PAPER

Pulsed-accelerated-flow studies of the temperature dependence of fast reactions †

Robert H. Becker, Wenzel P. Bartlett,‡ Edward T. Urbansky § and Dale W. Margerum *

Department of Chemistry, Purdue University, West Lafayette, IN 47907-1393, USA.
E-mail: margerum@purdue.edu

Received 14th August 2001, Accepted 24th October 2001
First published as an Advance Article on the web 21st January 2002

A pulsed-accelerated-flow (PAF) spectrometer (model V) capable of non-ambient temperature studies of fast reaction kinetics is described. The PAF method uses accelerated flow mixing of reactants during short time periods to enable the resolution of mixing and reaction rate constants. A new mixing/observation cell and cell supports are designed to permit measurement of reaction kinetics from 40 °C to below 0 °C. The cell consists of two machined PEEK [(–$OC_6H_4OC_6H_4COC_6H_4$–)$_n$] pieces joined together to give an internal solution distribution system, which greatly reduces the number of connections needed compared to previous instruments to bring the reactants together. The reaction between $W(CN)_8^{4-}$ and $IrCl_6^{2-}$ in 0.50 M H_2SO_4 is studied at 0.0, 25.0, and 40.0 °C. Second-order rate constants of 0.650×10^8 M^{-1} s^{-1}, 1.05×10^8 M^{-1} s^{-1}, and 1.29×10^8 M^{-1} s^{-1} are obtained, respectively. These data give activation parameters of $\Delta H^{\ddagger} = 10.0 \pm 0.8$ kJ mol^{-1} and $\Delta S^{\ddagger} = -58 \pm 3$ J mol^{-1} K^{-1}. Activation parameters for reverse bromine hydrolysis ($HOBr + Br^- + H^+ \longrightarrow Br_2 + H_2O$) were determined from rate constants measured from 0.0 to 40.0 °C. These were used to calculate the activation parameters for the forward bromine hydrolysis ($\Delta H^{\ddagger} = 66 \pm 1$ kJ mol^{-1} and $\Delta S^{\ddagger} = 10 \pm 20$ J mol^{-1} K^{-1}). The temperature dependence of the extremely rapid BrCl hydrolysis reaction (in equilibrium with $BrCl_2^-$) is determined as well. For reactions at temperatures of 25.0 °C, 10.0 °C, and 0.0 °C the values are 3.3×10^6 s^{-1}, 2.06×10^6 s^{-1}, and 1.75×10^6 s^{-1}, respectively. These values correspond to activation parameters of $\Delta H^{\ddagger} = 15 \pm 7$ kJ mol^{-1} and $\Delta S^{\pm} = -71 \pm 24$ J mol^{-1} K^{-1} for BrCl hydrolysis.

Introduction

The use of continuous-flow methods to elucidate the kinetics of fast reactions was initiated many years ago.[1] Although stopped-flow techniques are much more widely used, continuous-flow mixing has inherent advantages for very fast reactions provided the chemical reaction rate and the physical mixing rate can be distinguished from one another. This has been accomplished by the use of pulsed-accelerated-flow (PAF) instruments where variable flow velocities permit the resolution of mixing rate constants and reaction rate constants during the mixing process.[2–6] The range of quantifiable reaction rate constants has been pushed to values as large as 500,000 s^{-1} ($t_{1/2}$ = 1.4 μs) for pseudo-first-order reactions.[6] The Margerum research group has made extensive use of several PAF instruments for the determination of many rate constants[7–9] that could not be obtained with stopped-flow or relaxation techniques. However, none of these instruments could measure kinetics at non-ambient temperatures.

The pulsed-accelerated-flow model V was constructed to permit measurements at different temperatures so that activation parameters could be determined. It uses the best aspects of earlier instrument designs and incorporates new ideas to enable it to operate from 40 °C to less than 0 °C. Making this non-ambient functionality possible is a redesigned reactant flow system. This system uses a novel approach to construct a new mixing/observation cell with cell supports in a thermostated bath for temperature control. The instrument was tested at 25.0 °C with the $W(CN)_8^{4-}/IrCl_6^{2-}$ system used for previous PAF calibrations.[5,6] Reaction rates at 0.0 °C and 40.0 °C were then measured to obtain the activation parameters, which had not been measured previously. The new instrument was then used to study the kinetics of reverse bromine hydrolysis and bromine chloride hydrolysis.

The PAF–V is based on a continuous flow model with integrating observation.[10] Eqn. (1) describes integrating observation, as absorbance changes are followed down the reaction tube, for first-order reactions.

$$M = \frac{A_v - A_\infty}{A_o - A_\infty} = \frac{1 - e^{-Y}}{Y} \quad \text{where} \quad Y = \frac{k_{app} b}{v} \qquad (1)$$

In eqn. (1), A_v represents the absorbance at any flow velocity v, A_∞ is the absorbance of the reaction at infinite time (the product absorbance), A_o is the overall absorbance of the reactant species, k_{app} is the apparent rate constant, and b is the reaction length (0.01025 m) in the cell. The apparent rate constant is composed of a mixing rate constant (k_{mix}) and a reaction rate constant (k_r), (eqn. (2)).

$$A + B \xrightarrow{k_{mix}} (A \cdot B)_{mix} \xrightarrow{k_r} P \qquad (2)$$

The mixing rate constant is equal to a mixing proportionality constant (k_m) times the velocity at which the mixing takes place ($k_{mix} = k_m v$).[4,11,12] These two constants are resolved by use of eqn. (3), which takes into account the velocity dependence of k_{mix}.

$$\frac{1}{k_{app}} = \frac{1}{k_m \cdot v} + \frac{1}{k_r} \qquad (3)$$

† Based on the presentation given at Dalton Discussion No. 4, 10–13th January 2002, Kloster Banz, Germany.
‡ Current address: Dow Chemical, Freeport, TX 77541, USA.
§ Current address: United States Environmental Protection Agency, National Risk Management Research Laboratory, Cincinnati, OH 45268, USA.

DOI: 10.1039/b107341a

With pseudo-first-order rate constants of 4,000 s^{-1} or greater, the e^{-Y} term in eqn. (1) becomes insignificant and eqn. (1) is simplified. Combining eqn. (3) with the simplified version of eqn. (1) yields eqn. (4), which is the *M* plot equation used when studying slower reactions (<70,000 s^{-1}). With faster reactions (>70,000 s^{-1}) a *c*/*v* correction is needed (eqn. (5)).[6]

$$M = \frac{v}{b \cdot k_r} + \frac{1}{b \cdot k_m} \quad (4)$$

$$M = \frac{c}{v} + \frac{v}{b \cdot k_r} + \frac{1}{b \cdot k_m} \quad (5)$$

The *c*/*v* correction accounts for the empirical observation that as k_r increases the mixing rate constant (k_{mix}) becomes proportional to the square of the flow velocity in the immediate vicinity of the mixing jets in the center of the cell. The extent of this contribution is negligible for smaller k_r values, where most of the reaction takes place in the flow tube and $k_{mix} \propto v$.[6] The value of *c* varies from data set to data set depending upon experimental conditions, and is evaluated from a linear-least squares treatment of the rapid reaction data.

The ability of the PAF–V to function at low temperatures is crucial for work in our laboratory concerning Arctic chemistry with respect to bromine-catalyzed ozone depletion. We, therefore, determined the temperature dependence of the reaction of $HOBr + Br^- + H^+$ to form Br_2 and H_2O (reverse bromine hydrolysis) (eqn. (6)) and of the hydrolysis of BrCl (eqn. (7)).

$$HOBr_{(aq)} + Br^- + H^+ \rightleftharpoons Br_2 + H_2O \quad (6)$$

$$BrCl_{(aq)} + H_2O \rightleftharpoons HOBr + Cl^- + H^+ \quad (7)$$

These reactions are critical steps in the Arctic sunrise ozone depletion mechanism developed by Vogt *et al.*[13] The high concentration of Cl^- in seawater permits rapid formation of BrCl(aq) (reverse reaction in eqn. (7)) as a faster pathway to the generation of Br_2 (through the BrCl/Br^- reaction).[9,13] The BrCl chemistry was recently studied,[9] but, using the PAF–V, the reaction rate constants at low temperatures are elucidated. This permits a more accurate comparison of halogen and interhalogen reactions at Arctic temperatures.

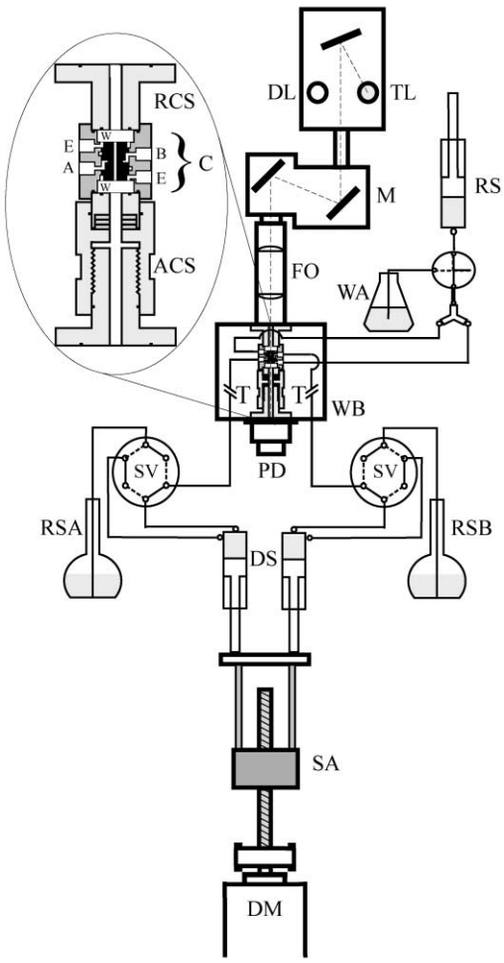

Fig. 1 Schematic of PAF–V. Key: DM, drive motor; SA, screw assembly; RSA, reactant solution A; RSB, reactant solution B; DS, drive syringes; SV, main switching valves; PD, photodetector; WB, water bath; WA, waste; FO, focusing optics; M, monochrometer; RS, receiving syringe; DL, deuterium lamp; TL, tungsten lamp; ACS, adjustable cell support; C, mixing/observation cell; W, quartz windows; A, reactant A entrance to cell; B, reactant B entrance to cell; E, product exit from cell; RCS, rigid cell support; T, a portion of the 4.6 m of coiled tubing not shown for clarity.

Experimental

Instrument design

Fig. 1 shows a schematic of the PAF–V design. The digital positioning system, filters, amplifiers, and data acquisition system, which were described previously,[6] are omitted from the figure for clarity. The PAF–V uses an Electro-craft PRO-400 programmable controller along with an Electro-craft MAX-400 amplifier to create specific velocity profiles, which are initiated by an Electro-craft E728 motor. The push system ramps the solution to a velocity of 13 m s^{-1}, within the cell, in a two-step process to minimize oscillations. Then it holds that velocity for 0.038 s, before beginning the decelerated portion of the push. The entire push lasts for 0.50 s. During the push, the drive motor (DM) turns the screw assembly (SA), which pushes 6 mL each of reactant solutions A and B (RSA, RSB) from the drive syringes (DS). The drive syringes are kept at room temperature to avoid thermal contraction leaking problems. The two solutions are pushed through the two main switching valves (SV) (UpChurch Scientific), and through 4.6 m of 0.1575 cm inner-diameter PEEK (polyetheretherketone) tubing (UpChurch). Most of the PEEK tubing (enough to hold 1.2 pushes worth of reactant solution) lies coiled within the 15 cm × 15 cm × 15 cm well-stirred thermostated bath (WB) (long length of tubing not shown in Fig. 1 for clarity (T)). This enables the reactant solutions in the tubing to reach thermal equilibrium with the bath before being mixed in the cell. The time required for temperature equilibrium establishment at 0 °C, from 25 °C solutions, is 10–20 s. The two reactant solutions enter into, and are distributed through, the twin-reaction path mixing/observation cell (C). (Further details of solution distribution within the cell are given below.) A space of 0.025 cm between the inner cylinder and the quartz window (W) at each end of the cell provides a path for the mixed solution to flow to the exits (E). After exiting the cell, the solution flows into a Gastight® receiving syringe (Hamilton) (RS). The PAF–V incorporates UV (30 W deuterium) and visible (50 W tungsten) lamps (DL, TL). Radiation passes from the lamps into a dual-grating monochrometer (Instruments, SA: DH-10; 200–800 nm; 250 nm blaze concave holographic gratings) (M), and through a set of focusing optics (FO), which focus the light at the center of the cell. Absorbance change detection occurs along the long axis of the cell with a photodetector (Semiconductor Circuits, Inc.) (PD). A total of 250 absorbance *vs.* velocity (13 to 3 m s^{-1}) data points are collected per push, and analyzed with three computer programs written in this laboratory. The Capture program[4] collects the data from the PAF. Data analysis is performed off-line by EZFilter[14] and NWPCalc.[15] EZFilter takes the raw Capture data and displays it in a LabVIEW format.[16] This program allows for easy data exploration and averaging. NWPCalc is then used to obtain the desired rate constant.

In order to operate the PAF–V at non-ambient temperatures, the instrument's thermostated bath, cell supports, and cell were redesigned and all were constructed from PEEK. This ensures that all pieces of the instrument, exposed to the variable temperatures, would expand and contract to the same extent to avoid any leaking of reactant solutions due to different coefficients of thermal expansion. PEEK was chosen for all pieces because of its commercial availability, ease of machining and appreciable coefficient of thermal expansion (2×10^5 K^{-1}).[17] The new thermostated bath facilitates easier cell installation and removal. This bath is insulated with black foam rubber to allow for cold temperature studies. The cell supports were designed for easy installation within the bath. Positioning of the cell, with hand tightening of the adjustable cell support (ACS), against the rigid cell support (RCS) holds the cell tightly during pushes. The adjustable cell support, shown in the enlarged part of Fig. 1, is composed of four separate pieces. The two lowest pieces of the adjustable cell support allow for increasing/decreasing of the length of that piece to tighten the cell in place. The other two pieces shown are the steel ball bearings and a PEEK cover for those bearings. These keep the cell stationary while the instrument operator tightens or loosens the adjustable cell support. Machining the inner diameters of all cell support pieces to 1.27 cm decreased the amount of light reflecting off the machined PEEK inner surfaces and allows for better data acquisition.

PAF cell

Previous PAF instruments used a single piece of PVC for twin-path mixing cell construction. This cell had an outside diameter of 38 mm with ten inlets, for the introduction of reactant solutions, that permitted flow to the center of the cell. The diameter of the inlets was reduced stepwise to 0.33 mm before they converged to form a 10-jet mixer at the center of the mixing/observation cell. Previous PAF instruments used two distribution blocks to deliver the reactant solutions from the drive syringes to the cell. Each block equally divided the reactant into five tubes, which connected to the mixing/observation cell. These ten tubes were placed radially in alternating positions around the PAF cells. This design required a total of 22 connections within the thermostated bath. Leaking from the 22 connectors that held the tubes was a frequent problem that increased with deviation from ambient temperature.

In the new design, for the PAF–V, the cell is constructed of two pieces (Fig. 2A), an inner cylinder and an outer sleeve, both made from PEEK. The outer sleeve has two solution-inlet screw holes (A and B), two exit screw holes (not shown in Fig. 2), and two solution channels cut into the inside of the sleeve. The inner cylinder has ten alternating grooves (pointing in opposite directions along the long axis of the cell) each with a small, slightly tapered, conical outlet that leads into the center of the cylinder. Together, these outlets act as a ten-jet mixer (Fig. 2B). The outer sleeve has an open inner diameter, for the inner cylinder, that is slightly smaller than the diameter of the inner cylinder. To join the two pieces, the outer sleeve is heated in boiling water to expand the PEEK while the inner cylinder is cooled in a dry-ice/acetone bath to contract it. The inner cylinder is carefully inserted into the outer sleeve and held in position until the two come to thermal equilibrium. Once equilibrium is established, the two pieces are firmly set and do not shift with respect to one another under PAF working conditions.

The new cell allows for internal solution distribution, this negates the need for distribution blocks as with previous PAF models. Solutions are distributed 360 degrees around the inner channel of the outer sleeve and then pushed into the ten alternating grooves of the inner cylinder (five grooves per reagent). The top grooves in Fig. 2A receive solution A and the bottom grooves receive solution B. The two solutions then move into the ten inlet jet channels and mix at the center of the cell. Once

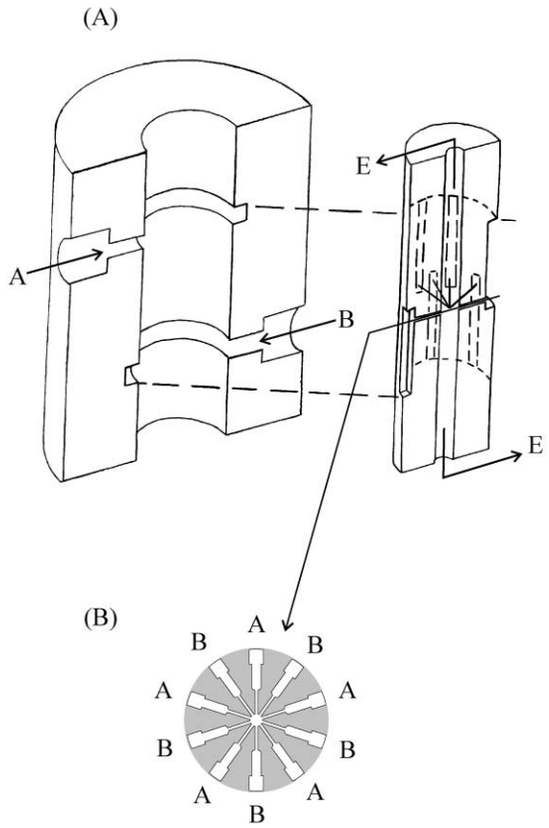

Fig. 2 (A) Cut-away of new twin-path PAF mixing/observation cell. The cell is composed of two pieces, an outer sleeve and an inner cylinder. The cell allows for internal solution distribution. Reactants (A and B) are distributed around the channels in the outer sleeve and are pushed into ten alternating grooves, and then into ten channels that form the ten-jet mixer. Product solution flows in two directions along the long axis of the cell to the exits (E). (B) Overhead view of the 10-jet mixer.

mixed, the reacting solution flows in opposite directions down the center of the cell (1.4 mm diameter twin observation path) and out towards the two exits (E). This gives an optical path of 2.050 cm, while the twin reaction paths are 1.025 cm. Two UV transparent quartz windows (0.635 cm thick, 1.905 cm diameter, (W) in Fig. 1, and not shown in Fig. 2A) hold the solution in the cell as it travels in two directions towards the exits.

Reagents

All solutions were made with distilled-deionized water. Solutions were either boiled or purged with Ar to remove CO_2 contamination. All solutions were filtered through 0.45 μm Millipore filter paper and degassed under aspiration and agitation for one hour. The degassing procedure is stopped when no air bubbles evolve from continued aspiration. Spectrophotometric measurements were made on a Perkin-Elmer Lambda-9 UV/vis/NIR spectrophotometer. An Orion Model 720A digital pH meter, equipped with Corning combination electrodes was used for pH determinations. pH values were corrected to $p[H^+]$ based on electrode calibration with standardized NaOH and $HClO_4$ as a function of ionic strength.

$Na_2IrCl_6 \cdot 6H_2O$ was used as received (Aldrich 99.9+%). Iridium solution concentrations were determined spectrophotometrically ($\varepsilon_{487} = 4075$ M^{-1} cm^{-1}).[18] $K_4W(CN)_8$ was prepared by the method of Leipoldt,[19] and was recrystallized from water and ethanol. Solution concentrations were determined both by titration with primary-standard-grade $(NH_4)Ce(NO_3)_6$ with ferroin as the indicator, and by spectrophotometric methods ($\varepsilon_{268} = 262$ M^{-1} cm^{-1}). Tungsten/iridium reactions were run in 0.5 M H_2SO_4. $W(CN)_8^{4-}$ is relatively stable in this acid medium, but decomposes in light.

For reverse bromine hydrolysis studies, ionic strength was held at 0.5 M by addition of $NaClO_4$, which was prepared from the recrystallized salt, and standardized gravimetrically. Aqueous bromine solutions (HOBr) were prepared with the addition of Br_2 (l). All bromine solutions were protected from ambient light and air. HBr solutions were prepared from titrimetrically standardized $HClO_4$ and from gravimetrically standardized, recrystallized NaBr. The $p[H^+]$ of the HOBr solutions was adjusted to 6–7 by the addition of a small amount of NaOH. Spectrophotometric measurements were made within ten minutes of solution preparation to avoid significant HOBr disproportionation. After equilibrium measurements of the HOBr solutions were made, a small amount of 70% $HClO_4$ was added following the method developed by Beckwith *et al.*[20] to determine total bromine. For the reverse bromine hydrolysis reaction, pseudo-first-order conditions were used with HOBr as the limiting reagent (eqn. (8)), where $k_{obsd} = k_6[H^+][Br^-]$. The production of a small amount of Br_3^- was followed at 266 nm ($\varepsilon = 40{,}900\ M^{-1}\ cm^{-1}$).[21]

$$\frac{d[Br_2(aq)]}{dt} = k_{obsd}[HOBr] \qquad (8)$$

For BrCl hydrolysis, aqueous solutions of BrCl were prepared by dissolving stoichiometric amounts of NaBr and $NaBrO_3$ with 6 M HCl. This solution was allowed to react for approximately one day, and then Br^--free NaCl was added. Br^--free NaCl was prepared from Br^--free HCl and saturated NaOH. The Br^--free HCl was prepared by diluting concentrated HCl to 20%. A mass of 0.5 g of $KMnO_4$ was added, and the solution (approx. 1500 mL) was boiled for one hour to remove trace iodide and bromide species that were converted to Br_2 and I_2 and volatilized. HCl was then distilled for use.[22] Phosphate buffer solutions were prepared in a 4 : 5 to 1 : 5 ratio of NaH_2PO_4 to Na_2HPO_4, respectively, and adjusted to a $p[H^+]$ of 6.6 with standardized NaOH. All solutions in this study were 2.0 M in $[Cl^-]$. This high concentration suppresses the BrCl hydrolysis reaction rate.[9] The hydrolysis of BrCl is followed at 232 nm by observing the loss of $[BrCl]_{total}$ (where $[BrCl]_{total} = [BrCl] + [BrCl_2^-]$).

Results and discussion

Temperature study of tungsten(IV)/iridium(IV) reaction

The reaction between octacyanotungstate(IV) and hexachloroiridate(IV) (eqn. (9)) has been used as a calibration reaction for previous PAF instruments.[5,6]

$$W(CN)_8^{4-} + IrCl_6^{2-} \longrightarrow W(CN)_8^{3-} + IrCl_6^{3-} \qquad (9)$$

The system is fast enough to study a wide range of pseudo-first-order (tungsten in excess) reaction rates over a wide temperature range. The loss in absorbance of $IrCl_6^{2-}$ is followed at 487 nm. Fig. 3 is an example of data collected for the $W(CN)_8^{4-}/IrCl_6^{2-}$ reaction at 0.0 °C (the data are an ensemble of five pushes). The graph of *M vs.* velocity (from eqn. (4)) for 250 data points is shown. Fig. 4 shows data collected for this reaction at 25.0 °C. The second-order-rate constant for this reaction is $(1.05 \pm 0.03) \times 10^8\ M^{-1}\ s^{-1}$. This is in close agreement to that determined by previous PAF instruments.[5,6] Fig. 4 also shows tungsten/iridium reaction data at temperatures of 40.0 °C and 0.0 °C. The second-order rate constants for these two temperatures are $(1.29 \pm 0.08) \times 10^8\ M^{-1}\ s^{-1}$ and $(0.650 \pm 0.007) \times 10^8\ M^{-1}\ s^{-1}$, respectively (Table 1). The high ionic strength (0.50 M) used for these studies shields much of the electrostatic repulsion between the reactants. Calculations, considering temperature, ionic strength, and charged species, show that the rates are slower than diffusion controlled processes.[23] Even at 40.0 °C the diffusion-controlled rate constant is an order of magnitude greater than the measured second-order rate constant.[23]

Table 1 Temperature dependence of the reaction rate constants studied on PAF–V

Reaction	*T*/°C	Resolved rate constant
Reverse bromine hydrolysis	0.0	$(1.48 \pm 0.06) \times 10^{10}\ M^{-2}\ s^{-1}$
	7.0	$(1.56 \pm 0.03) \times 10^{10}\ M^{-2}\ s^{-1}$
	15.0	$(1.59 \pm 0.06) \times 10^{10}\ M^{-2}\ s^{-1}$
	25.0	$(1.70 \pm 0.09) \times 10^{10}\ M^{-2}\ s^{-1}$
	32.0	$(1.96 \pm 0.07) \times 10^{10}\ M^{-2}\ s^{-1}$
	40.0	$(2.1 \pm 0.1) \times 10^{10}\ M^{-2}\ s^{-1}$
BrCl hydrolysis	0.0[a]	$(1.75 \pm 0.05) \times 10^6\ s^{-1}$
	10.0[b]	$(2.06 \pm 0.05) \times 10^6\ s^{-1}$
	25.0[c]	$(3.3 \pm 0.7) \times 10^6\ s^{-1}$
$W(CN)_8^{4-}/IrCl_6^{2-}$	0.0	$(0.650 \pm 0.007) \times 10^8\ M^{-1}\ s^{-1}$
	25.0	$(1.05 \pm 0.03) \times 10^8\ M^{-1}\ s^{-1}$
	40.0	$(1.29 \pm 0.08) \times 10^8\ M^{-1}\ s^{-1}$

[a] k_{obsd} measured on PAF–V for this temperature is $(1.46 \pm 0.05) \times 10^5\ s^{-1}$ where $K_{10} = 5.48\ M^{-1}$. [b] k_{obsd} measured on PAF–V for this temperature is $(2.00 \pm 0.05) \times 10^5\ s^{-1}$ where $K_{10} = 4.65\ M^{-1}$. [c] k_{obsd} measured on PAF–V for this temperature is $(3.8 \pm 0.8) \times 10^5\ s^{-1}$ where $K_{10} = 3.8\ M^{-1}$.

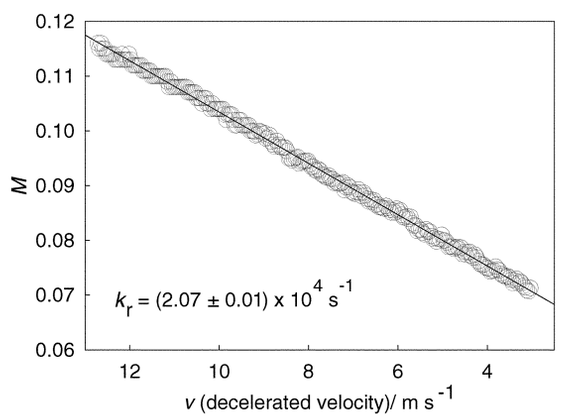

Fig. 3 PAF–V kinetic *M*-plot data of $W(CN)_8^{4-}/IrCl_6^{2-}$ reaction at 0.0 °C. This graph represents five ensemble data pushes. Two hundred fifty *M vs.* velocity data points taken during a reaction push. Slope equals $1/bk_r$. Post mixing, $[W(CN)_8^{4-}] = 3.22 \times 10^{-4}$ M, $[IrCl_6^{2-}] = 3.7 \times 10^{-5}$ M in 0.5 M H_2SO_4.

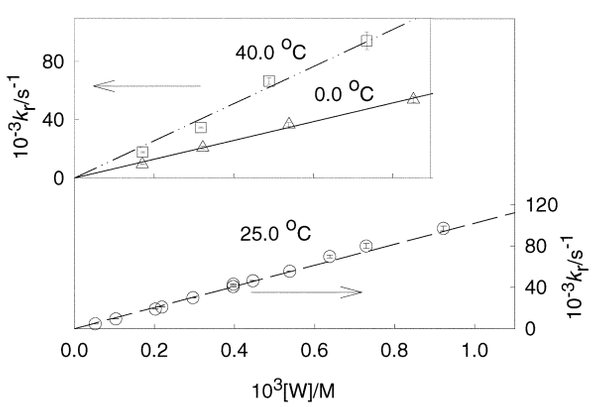

Fig. 4 PAF–V data for the reaction between $W(CN)_8^{4-}$ and $IrCl_6^{2-}$. Data for reactions studied at 0 °C, 25 °C, and 40 °C. Conditions: 0.5 M H_2SO_4 medium, $4 \times 10^{-5}\ M < [W] < 1 \times 10^{-3}$ M. Solid and dotted lines show the best fit of the individual temperature data. Second-order rate constants: 0 °C = $(0.650 \pm 0.007) \times 10^8\ M^{-1}\ s^{-1}$, 25 °C = $(1.05 \pm 0.03) \times 10^8\ M^{-1}\ s^{-1}$, and 40 °C = $(1.29 \pm 0.08) \times 10^8\ M^{-1}\ s^{-1}$.

A plot of $\ln(k/T)$ *vs.* $1/T$ for the tungsten(IV)/iridium(IV) second-order-rate constants (Fig. 5) yields $\Delta H^{\ddagger} = 10.0 \pm 0.8$ kJ mol^{-1}, and $\Delta S^{\ddagger} = -58 \pm 3$ J mol^{-1} K^{-1}.[23] The large negative $\Delta S^{\ddagger}$ is consistent with the loss of translational entropy in the transition state, due to solvent and counter ion association with the highly charged negative ion species.

Table 2 Summary of rate constants and activation parameters

Reaction	k_r'(25 °C)[a]	$\Delta H^{\ddagger}$/kJ mol^{-1}	$\Delta S^{\ddagger}$/J mol^{-1} K^{-1}
Cl_2 Hydrolysis[24]	22.3(6) s^{-1}	63(2)	−8(4)
Br_2 Hydrolysis[b,20]	97(7) s^{-1}	66(1)	10(20)
BrCl Hydrolysis[b]	3.3(7) × 10^6 s^{-1}	15(7)	−71(24)
Reverse Cl_2 Hydrolysis[24]	2.14(8) × 10^4 M^{-2} s^{-1}	27(1)	−71(9)
Reverse Br_2 Hydrolysis[b]	1.70(9) × 10^{10} M^{-2} s^{-1}	3.8(9)	−36(3)
$IrCl_6^{2-}/W(CN)_8^{4-}$[b]	1.05(3) × 10^8 M^{-1} s^{-1}	10.0(8)	−58(3)

[a] k_r' = resolved rate constant. [b] This work.

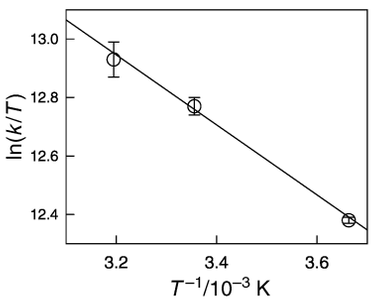

Fig. 5 Eyring plot for tungsten/iridium reaction temperature study. Activation parameters: $\Delta H^{\ddagger}$ = 10.0 ± 0.8 kJ mol^{-1}, $\Delta S^{\ddagger}$ = −58 ± 3 J mol^{-1} K^{-1}.

Reverse bromine hydrolysis

A previous study in our laboratory,[20] using the PAF–IV, gave (1.6 ± 0.2) × 10^{10} M^{-2} s^{-1} at 25.0 °C and μ = 0.5 M as the third-order rate constant for reverse bromine hydrolysis. Using the PAF–V, this reaction was repeated, and a value of (1.70 ± 0.09) × 10^{10} M^{-2} s^{-1} is obtained, which is in excellent agreement with the previous value. Table 1 lists the obtained rate constants for the reaction of reverse bromine hydrolysis at different temperatures. Plotting ln(k/T) *vs.* 1/T for this reaction gives an Eyring plot as shown in Fig. 6. The activation parameters for

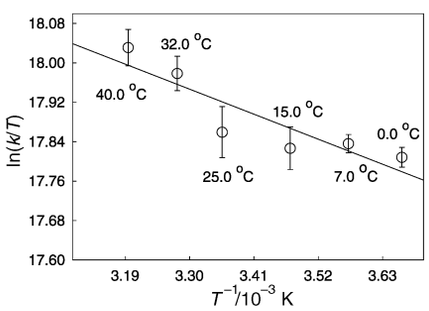

Fig. 6 Eyring plot for the reverse bromine hydrolysis temperature study. Activation parameters: $\Delta H^{\ddagger}$ = 3.8 ± 0.9 kJ mol^{-1}, $\Delta S^{\ddagger}$ = −36 ± 3 J mol^{-1} K^{-1}.

this reaction are $\Delta H^{\ddagger}$ = 3.8 ± 0.9 kJ mol^{-1} and $\Delta S^{\ddagger}$ = −36 ± 3 J mol^{-1} K^{-1}. The significant error in these values is due to the small change in observed rate constant with temperature for this reaction. As with chlorine hydrolysis,[24] we might expect a non-zero $\Delta C_p^{\ddagger}$ term for the reverse bromine hydrolysis system. However, due to scatter in the Eyring plot for the reverse reaction, values for $\Delta C_p^{\ddagger}$ are not reliable.[23] A comparison of the activation parameters for the reverse bromine hydrolysis reaction to that of reverse chlorine hydrolysis[24] ($\Delta H^{\ddagger}$ = 27 ± 1 kJ mol^{-1} and $\Delta S^{\ddagger}$ = −71 ± 9 J mol^{-1} K^{-1}) shows that $\Delta H^{\ddagger}$ is much smaller for the bromine species. The smaller $\Delta S^{\ddagger}$ suggests less water coordination in the transition state around the bromine species. The use of values obtained in this study, and ΔH° = 62 ± 1 kJ mol^{-1} and ΔS° = 46 ± 5 J mol^{-1} K^{-1} from Beckwith *et al.*,[20] enabled the calculation of the activation parameters for the forward bromine hydrolysis reaction ($\Delta H^{\ddagger}$ = 66 ± 1 kJ mol^{-1} and $\Delta S^{\ddagger}$ = 10 ± 20 J mol^{-1} K^{-1}). These values are consistent with those for forward chlorine hydrolysis, which is of comparable rate, but much different than those obtained in a BrCl hydrolysis study.

BrCl hydrolysis

Liu *et al.*[9] recently studied the equilibrium and kinetics of bromine chloride hydrolysis by use of the PAF–IV instrument at 25.0 °C. An observed first-order-rate constant of (3.5 ± 0.5) × 10^5 s^{-1} was obtained. In the 2.0 M chloride-ion solutions used for the study, only a small percentage of $[BrCl]_{total}$ exists as BrCl and most is in the form of $BrCl_2^-$ (eqn. (10)).[9]

$$BrCl + Cl^- \underset{}{\overset{K_{10}}{\rightleftharpoons}} BrCl_2^- \qquad (10)$$

This enabled Liu *et al.* to slow the reaction to a rate observable with the PAF–IV. The true first-order-rate constant (after correction for $BrCl_2^-$) is (3.0 ± 0.4) × 10^6 s^{-1}. This study was also conducted on the PAF–V. At 25.0 °C a BrCl hydrolysis rate constant of (3.3 ± 0.7) × 10^6 s^{-1} was obtained, after correcting for the equilibrium in eqn. (10), which is within the error of that obtained by Liu and Margerum.[9] Rate constants at 10.0 °C and 0.0 °C are (2.06 ± 0.05) × 10^6 s^{-1} and (1.75 ± 0.05) × 10^6 s^{-1}, respectively, after taking into consideration the shift in $BrCl_2^-$/BrCl equilibrium with temperature (Table 1).[9] With the three temperature values, activation parameters of $\Delta H^{\ddagger}$ = 15 ± 7 kJ mol^{-1} and $\Delta S^{\ddagger}$ = −71 ± 24 J mol^{-1} K^{-1} were obtained.

A comparison of the activation parameters of the much faster BrCl hydrolysis reaction to those of bromine and chlorine[24] hydrolysis shows a large difference in values. For Cl_2 hydrolysis $\Delta H^{\ddagger}$ = 63 ± 2 kJ mol^{-1} and for Br_2 hydrolysis $\Delta H^{\ddagger}$ = 66 ± 1 kJ mol^{-1} as compared to the value of 15 ± 7 kJ mol^{-1} for BrCl hydrolysis. The $\Delta S^{\ddagger}$ for BrCl is much more negative than values for bromine and chlorine.[24] The dipole in BrCl helps water to associate with the molecule and lowers the enthalpic energy ($\Delta H^{\ddagger}$) of the transition state on the path to products in eqn. (7). Solvent association also affects the $\Delta S^{\ddagger}$ value, which is more negative than is the case for Br_2 and Cl_2 hydrolysis. However, the $\Delta H^{\ddagger}$ term dominates and the BrCl hydrolysis is 4–5 orders of magnitude faster than the Br_2 or Cl_2 hydrolysis.

Conclusion

A new instrument is described that allows collection of kinetic data for very fast chemical reactions at non-ambient temperatures. A new mixing/observation cell and cell supports are key to the proper function of the instrument at these temperatures. With this instrument, several rate constants are obtained, as well as activation parameters. Table 2 lists these values and also gives values, for comparison, of chlorine hydrolysis, reverse chlorine hydrolysis, and bromine hydrolysis obtained elsewhere.[24]

Acknowledgements

This work was supported by National Science Foundation Grants CHE-98–18214 and ATM-9631572.

References

1 H. Hartridge and F. J. W. Roughton, *Proc. R. Soc. London, Ser. A.*, 1923, **104**, 376.
2 G. D. Owens and D. W. Margerum, *Anal. Chem.*, 1980, **52**, 91A.
3 G. D. Owens, R. W. Taylor, T. Y. Ridley and D. W. Margerum, *Anal. Chem.*, 1980, **52**, 130.
4 S. A. Jacobs, M. T. Nemeth, G. W. Kramer, T. Y. Ridley and D. W. Margerum, *Anal. Chem.*, 1984, **56**, 1058.
5 M. T. Nemeth, K. D. Fogelman, T. Y. Ridley and D. W. Margerum, *Anal. Chem.*, 1987, **59**, 283.
6 C. P. Bowers, K. D. Fogelman, J. C. Nagy, T. Y. Ridley, Y. L. Wang, S. W. Evetts and D. W. Margerum, *Anal. Chem.*, 1997, **69**, 431.
7 M. R. McDonald, T. X. Wang, M. Gazda, W. M. Scheper, S. W. Evetts and D. W. Margerum, *Anal. Chem.*, 1997, **69**, 3513.
8 C. P. Bowers, K. D. Fogelman, J. C. Nagy, T. Y. Ridley, Y. L. Wang, S. W. Evetts and D. W. Margerum, *Anal. Chem.*, 1997, **69**, 431 and references therein; R. M. Liu and D. W. Margerum, *Inorg. Chem.*, 1998, **37**, 2531; Y. Xie, M. R. McDonald and D. W. Margerum, *Inorg. Chem.*, 1999, **38**, 3938; Z. Jia, M. G. Salaita and D. W. Margerum, *Inorg. Chem.*, 2000, **39**, 1974; Q. Liu, L. M. Schurter, C. E. Muller, S. Aloisio, J. S. Francisco and D. W. Margerum, *Inorg. Chem.*, 2001, **40**, 4436.
9 Q. Liu and D. W. Margerum, *Environ. Sci. Technol.*, 2001, **35**, 1127.
10 H. Gerisher and W. Z. Heim, *Z. Phys. Chem. (Frankfurt)*, 1965, **46**, 345.
11 H. Gerischer, J. Holzwarth, D. Seifert and L. Strohmaier, *Ber. Bunsen-Ges. Phys. Chem.*, 1969, **73**, 952.
12 H. L. Toor and M. Singh, *Ind. Eng. Chem. Fundam.*, 1973, **12**, 448.
13 R. Vogt, P. J. Crutzen and R. Sander, *Nature (London)*, 1996, **383**, 327.
14 W. P. Bartlett, M.S. Thesis, Purdue University, 1999.
15 K. D. Fogelman, Ph.D. Thesis, Purdue University, 1990; T. X. Wang, Ph.D. Thesis, Purdue University, 1994.
16 LabVIEW version 5.01; National Instruments, Austin, TX, 2000.
17 R. Khol, *Mach. Des.*, 1987, **59**, 8, 146.
18 C. K. Jorgenson, *Mol. Phys.*, 1959, **2**, 309.
19 J. G. Leipoldt, L. D. C. Bok and P. J. Z. Cilliers, *Anorg. Allg. Chem.*, 1974, **407**, 350.
20 R. C. Beckwith, T. X. Wang and D. W. Margerum, *Inorg. Chem.*, 1996, **35**, 995.
21 T. X. Wang, M. D. Kelley, J. N. Cooper, R. C. Beckwith and D. W. Margerum, *Inorg. Chem.*, 1994, **33**, 5872.
22 Z. Jia and D. W. Margerum, *Inorg. Chem.*, 1999, **38**, 5374.
23 J. H. Espenson, *Chemical Kinetics and Reaction Mechanism*, McGraw-Hill, New York, 1995, ch. 7, 9.
24 T. X. Wang and D. W. Margerum, *Inorg. Chem.*, 1994, **33**, 1050.